ISSN 0853-2982

JURNAL TEKNIK SIPIL
Jurnal Teoretis dan Terapan Bidang Rekayasa Sipil

3D Nonlinear Parallel FEM for Analyzing Dynamic Response of the Large-Scale Saturated Soil Layers-Civil Structures Interaction Problem (Part II: Validation and Performance)

Jafril Tanjung

Civil Engineering Department, Engineering Faculty, Andalas University, Padang
E-mail: jafriltanjung@ft.unand.ac.id, jafril_tanjung@yahoo.com

Abstract

In this second paper, a validation and performance of the nonlinear parallel FEM proposed in the first paper are evaluated. An experimental model for investigating a seismic earth pressure has been simulated for numerically validation purpose. The numerical results for the seismic active earth pressure parameters and dynamic pore water pressure acting on the wall coincide well with those of the experiment. The efficiency of the parallel computation was made clear by the comparison of the executing time for the different size of models. The results in this numerical analysis suggests the relation between the seismic active earth pressure and the dynamic pore water pressure acting on the wall for a saturated soil layer.

Keywords: *3D nonlinear FEM, parallel computation, domain decomposition method, saturated soil layers-civil structure interaction problem, dynamic earth pressure.*

Abstrak

Dalam makalah kedua ini akan dievaluasi keabsahan dan kinerja paralel elemen hingga non-linier yang dijabarkan dalam makalah pertama. Untuk maksud tersebut, model eksperimental untuk menganalisis perilaku seismik tekanan tanah, telah disimulasikan. Hasil analisis numerik menunjukkan bahwa nilai parameter seismik untuk tekanan tanah dan tekanan dinamik air pori yang bekerja pada dinding penahan tanah, sesuai dengan yang diamati dalam pengujian laboratorium. Efisiensi komputasi secara paralel ditunjukkan dengan membandingkan waktu yang diperlukan untuk menganalisis beberapa model dengan ukuran yang berbeda. Hasil analisis juga memberi gambaran tentang hubungan antara tekanan seismic tanah dan tekanan air pori yang bekerja pada dinding penahan lapisan tanah jenuh.

Keywords: *Metode elemen hingga non-linier 3-dimensi, paralel komputasi, metode dekomposisi domain, masalah interaksi antara lapisan tanah jenuh dan struktur sipil, analisis tekanan dinamik lapisan tanah.*

1. Introduction

A detail formulation of 3D nonlinear parallel FEM has been derived in fist paper (Tanjung, 2010). The formulation applied the Domain Decomposition Method (DDM) to separate a whole of analytical domain into several non-overlapping subdomains. By DDM, a boundary value problem was converted into an interface problem. An iterative Conjugate Gradient (CG) algorithm was used to solve its interface problem.

The proposed parallel FEM algorithm was implemented as a Single Program Multiple Data (SPMD) programming model and coded using FORTRAN-77 (Silverio, 1994). By this programming model, each processor will executes the same code asynchronously without communicating each other. The synchronization takes place only when processors need to exchange data in order to obtain the solution of the interface problem. The interprocessor communication based on the hypercube networking was constructed and performed in the message-passing paradigm by using the PVM programming libraries (Geist, 1996) as a parallel interpreter.

Two types of analysis were conducted to validate and to evaluate performance of this proposed 3D nonlinear parallel FEM described in the first paper. At first, an experimental model based on Kawamura's work (1979) was simulated. The validation of this proposed parallel algorithm was achieved by comparing the analysis results to these experimental works. Furthermore, the performance of current parallel algorithm was evaluated based on analysis results of the models

with different number of elements and subdomains. Computer memory requirement and elapsed computation time were used as performance indicators in this study.

2. Analytical Model

2.1 Experiment and FEM Model

The experimental model simulated in this study is a shaking table test for investigating the dynamic active earth pressure and the dynamic response of pore water pressure in saturated soil layer. The experiment model was contained Toyoura sand as the backfill soil. When preparing the experimental model, the soil backfill was contained every 10 cm deep in a steel box, partially filled with the water and compacted to obtain the backfill soil in moderately dense condition. The dimensions of the steel box are 100 cm high, 200 cm long and 100 cm wide. The height of the saturated backfill soil was 56 cm. The box was horizontally shaken by a pure sinusoidal excitation with frequency of 3 Hz and constant amplitude of 300 gals. One side of the box was equipped with a steel wall. The wall was allowed to move outward during the excitation. The pressures acting on the wall were measured using the load cells as notated P in **Figure 1**. The velocity of the wall movement in the horizontal direction is 0.02 mm/sec. Movement of the wall was measured at the middle of the wall height as shown in **Figure 2**. Pore water pressures were measured using pore water pressure cells attached to the surface of the moveable wall.

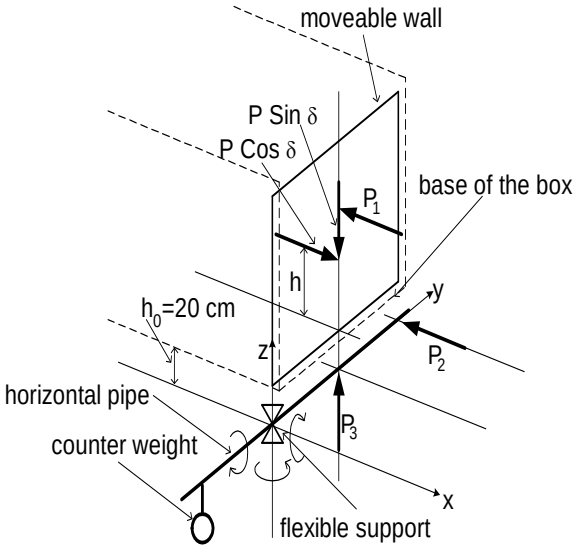

Figure 1. Setup of the Experimental Model

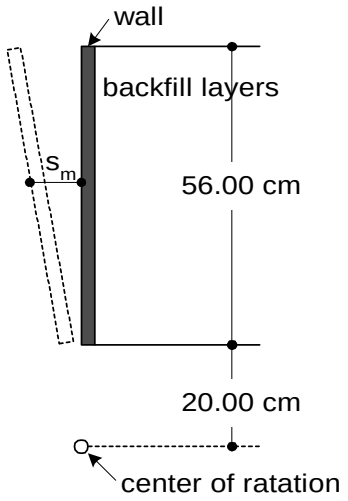

Figure 2. Illustration of the Wall Movement

A model for the numerical analysis was prepared in the same size with the experimental model. A wall located on the one side of the model was also allowed to move outward during excitation. Movement of the wall was controlled such that horizontally moving with velocity 0.02 mm/second. Meshing of analytical model is shown in **Figure 3**. The model was divided into eight non-overlapping subdomains, assigned to eight processors and parallelly solved by eight processors. To maintain the continuity conditions on the interfaces' subdomains, the subdomains were linked using the interface nodes as marked in bold dashed lines in **Figure 3**. The numerical integration of Hilber -α method was applied with a constant time step Δt = 0.01 second. The parameter for the time integration $\overline{\alpha}$ was taken as –0.25 (Hughes, 1996). The damping ratio for soil grain was assumed as 0.05 (Ishihara, 1996). The final solution in each time step was confirmed when the convergence criterion $\varepsilon_c=10^{-4}$ was satisfied on the nonlinear iteration of the modified Newton-Raphson method (Press, 1995).

The initial condition for the pore water pressure was assumed hydrostatic. The coefficient of the earth pressure at rest, which is related to the initial condition for the effective stress, was specified as 0.6. Its value was taken based on fact that in the experiment work the backfill soil was artificially compacted to obtain a moderate dense condition. Except for the upper surface of the analytical model, both of the soil grains and the pore water were not allowed to move outward at the boundaries of the model. The pore water pressure on the upper surface of the model was kept equal to zero during analysis.

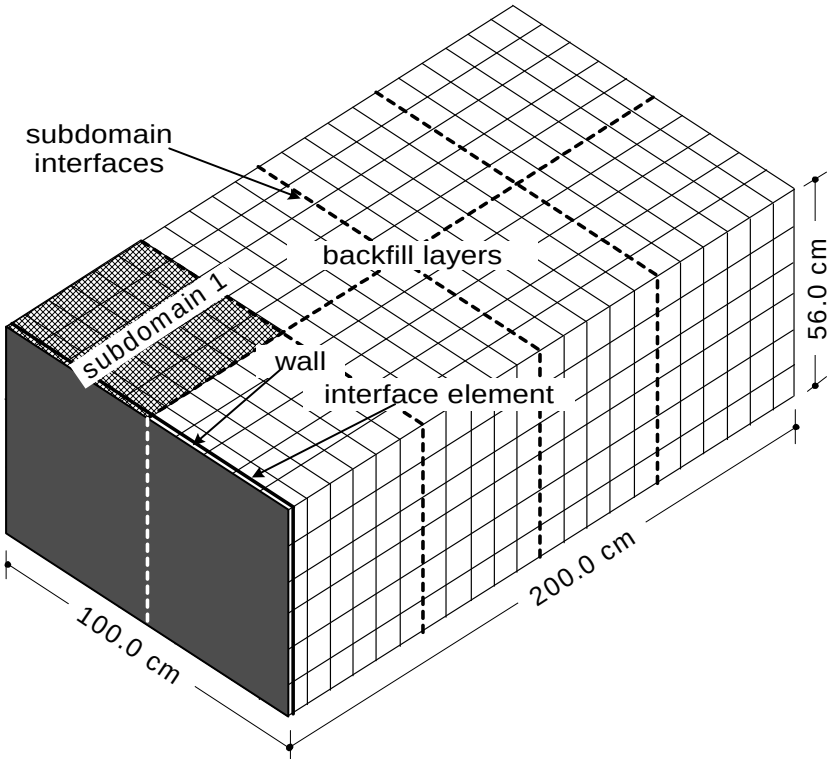

Figure 3. FEM Mesh of the Numerical Model

2.2 Moveable Wall Model

For analytical model, a moveable wall was represented by the moving boundary applied to the wall. The equation of motion used in finite element analysis was obtained by arranging **Equation (34)** in the first paper associated with the free unknown and moving boundary components. For a given a displacement increment on moveable wall nodes $\Delta\mathbf{d}_{(b)}^{(s)}$ **Equations (44)** and **(46)** in the first paper, may be rewritten as follow.

$$\hat{\mathbf{K}}_{T(ii)_n}^{(s)} = \frac{1}{\bar{\beta}\,\Delta t^2}\mathbf{M}_{(ii)}^{(s)} + \frac{\bar{\gamma}}{\bar{\beta}\,\Delta t}\mathbf{D}_{(ii)n-1}^{(s)} + \mathbf{K}_{T(ii)n-1}^{(s)} \quad (1)$$

$$\begin{aligned}\Delta\hat{\mathbf{F}}_{(i)n+1}^{(s)} = {} & \left(\mathbf{F}_{(i)n+1}^{(s)} - \mathbf{F}_{(i)n}^{(s)}\right) + \left(\frac{1}{\bar{\beta}\,\Delta t}\mathbf{M}_{(ii)}^{(s)} + \frac{\bar{\gamma}}{\bar{\beta}}\mathbf{D}_{(ii)n-1}^{(s)}\right)\dot{\mathbf{d}}_{(i)n}^{(s)} \\ & + \left(\frac{1}{2\bar{\beta}}\mathbf{M}_{(ii)}^{(s)} + \left(\frac{\bar{\gamma}}{2\bar{\beta}} - 1\right)\Delta t\ \mathbf{D}_{(ii)n-1}^{(s)}\right)\ddot{\mathbf{d}}_{(i)n}^{(s)} \\ & + \left(\frac{1}{\bar{\beta}\,\Delta t}\mathbf{M}_{(ib)}^{(s)} + \frac{\bar{\gamma}}{\bar{\beta}}\mathbf{D}_{(ib)n-1}^{(s)}\right)\dot{\mathbf{d}}_{(b)n}^{(s)} \\ & + \left(\frac{1}{2\bar{\beta}}\mathbf{M}_{(ib)}^{(s)} + \left(\frac{\bar{\gamma}}{2\bar{\beta}} - 1\right)\Delta t\ \mathbf{D}_{(ib)n-1}^{(s)}\right)\ddot{\mathbf{d}}_{(b)n}^{(s)} \\ & - \left(\frac{1}{\bar{\beta}\,\Delta t^2}\mathbf{M}_{(ib)}^{(s)} + \frac{\bar{\gamma}}{\bar{\beta}\,\Delta t}\mathbf{D}_{(ib)n-1}^{(s)} + \mathbf{K}_{T(ib)n-1}^{(s)}\right)\Delta\mathbf{d}_{(b)n}^{(s)}\end{aligned} \quad (2)$$

The indexes i and b denote the free unknown and the moveable degrees of freedom, respectively.

2.3 Joint Surface Element

In order to represent the discontinuous behaviour on the interface between backfill soil and moveable wall, the joint surface element which developed by Beer (1985) was adopted in this study. A configuration of the joint surface element in the global coordinate system (x,y,z) at its mapped area into local system (ξ,η) is shown in **Figure 4.** Contras to regular element, a definition of stresses for joint surface element are evaluated based on relative displacement between top and bottom surfaces element. These stresses and relative displacement are considered in normal and tangential directions to the surface. The stress-relative displacement relationship was defined referring the paper by Toki et al (1981).

For a known the displacement increment of nodes located on the top and bottom of surface at current time step, a relative displacement in global coordinate system $\bar{\mathbf{d}}$ can be defined as follow. Subscript n denotes the current time step is temporary omitted for simplification.

$$\bar{d}_x = \sum_{i=1}^{4} N_i(\xi,\eta)\left(\Delta d_{xi}^{top} - \Delta d_{xi}^{bottom}\right) \quad (3)$$

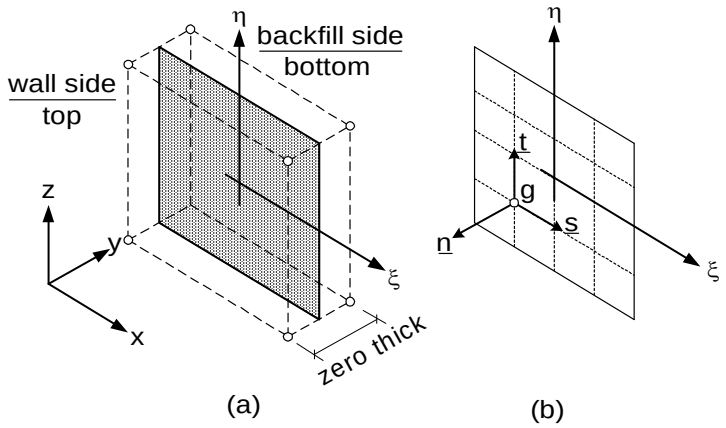

Figure 4. Joint Element (a) Configuration, (b) Mapped Area

$$\bar{d}_y = \sum_{i=1}^{4} N_i(\xi,\eta)\left(\Delta d_{yi}^{top} - \Delta d_{yi}^{bottom}\right) \quad (4)$$

$$\bar{d}_z = \sum_{i=1}^{4} N_i(\xi,\eta)\left(\Delta d_{zi}^{top} - \Delta d_{zi}^{bottom}\right) \quad (5)$$

Δd_{ji}^{top} and Δd_{ji}^{bottom} are the displacements increment of node i in coordinate direction j which is located on the top and bottom side of a joint surface element, respectively. N_i (ξ, η) is the shape function for surface element. The relative displacements for normal and tangential directions are obtained by transforming the relative displacement in global coordinate system into local coordinate system. For any gauss point g, the relative displacement is defined as follow.

$$\begin{Bmatrix} \bar{d}_n \\ \bar{d}_s \\ \bar{d}_t \end{Bmatrix}_g = \begin{bmatrix} n_x & n_y & n_z \\ s_x & s_y & s_z \\ t_x & t_y & t_z \end{bmatrix}_g \begin{Bmatrix} \bar{d}_x \\ \bar{d}_y \\ \bar{d}_z \end{Bmatrix} \quad (6)$$

In **Equation (6)**, notation n, s and t denote normal and tangential directions as shown in **Figure 4**. n_i, S_i and t_i are the components of the unit vector normal and tangential directions to the surface, respectively. These unit vectors are defined as in **Equation (7)**.

$$\{n\} = \frac{\{\bar{V}_\xi\}}{\left|\{\bar{V}_\xi\}\right|} \; ; \; \{t\} = \frac{\{\bar{V}_\xi\}\times\{\bar{V}_\eta\}}{\left|\{\bar{V}_\xi\}\right|\cdot\left|\{\bar{V}_\eta\}\right|} \; ; \; \{s\} = \{t\}\times\{n\} \quad (7)$$

$$\{\bar{V}_\xi\} = \begin{Bmatrix} \partial x/\partial\xi \\ \partial y/\partial\xi \\ \partial z/\partial\xi \end{Bmatrix} \; ; \; \{\bar{V}_\eta\} = \begin{Bmatrix} \partial x/\partial\eta \\ \partial y/\partial\eta \\ \partial z/\partial\eta \end{Bmatrix} \quad (8)$$

$$\frac{\partial x}{\partial\xi} = \sum_{i=1}^{4} \frac{\partial N_i(\xi,\eta)}{\partial\xi} x_i \; ; \; \frac{\partial x}{\partial\eta} = \sum_{i=1}^{4} \frac{\partial N_i(\xi,\eta)}{\partial\eta} x_i \quad (9)$$

$$\frac{\partial y}{\partial\xi} = \sum_{i=1}^{4} \frac{\partial N_i(\xi,\eta)}{\partial\xi} y_i \; ; \; \frac{\partial y}{\partial\eta} = \sum_{i=1}^{4} \frac{\partial N_i(\xi,\eta)}{\partial\eta} y_i \quad (10)$$

$$\frac{\partial z}{\partial\xi} = \sum_{i=1}^{4} \frac{\partial N_i(\xi,\eta)}{\partial\xi} z_i \; ; \; \frac{\partial z}{\partial\eta} = \sum_{i=1}^{4} \frac{\partial N_i(\xi,\eta)}{\partial\eta} z_i \quad (11)$$

x_i, y_i and z_i are the coordinates of the node i on the bottom surface of the element.

Finally, using a definition of the relative displacement written in **Equation (6)**, the incremental of normal and shear stresses for a joint surface element $\Delta\sigma_n$, $\Delta\tau_s$, and $\Delta\tau_\tau$, can be calculated following **Equation (12)**. In this study, the behaviour in the normal direction was assumed to be uncoupled with the tangential direction.

$$\begin{Bmatrix} \Delta\sigma_n \\ \Delta\tau_s \\ \Delta\tau_t \end{Bmatrix} = \begin{bmatrix} \bar{k}_n & 0 & 0 \\ 0 & \bar{k}_s & 0 \\ 0 & 0 & \bar{k}_t \end{bmatrix} \begin{Bmatrix} \Delta d_n \\ \Delta d_s \\ \Delta d_t \end{Bmatrix} \quad (12)$$

The constants $\bar{k}_n$ and $\bar{k}_s$ are the nonlinear function represent the behaviors of joint surface element. These values are equal to zero when separating occurs, otherwise they are set to initial elastic properties k_n and k_s. The sliding will take place when the shear stress reaches the yield shear stress τ_y defined by the Coulomb law written in **Equation (13)**. For sliding condition, a value of constant $\bar{k}_s$ is also taken to zero.

$$\tau_y = C - \left(\sigma_n - \sigma_t\right) \tan\phi \quad (13)$$

Parameters C and ϕ denote equivalent adhesion and friction angle defining the material properties for the joint surface element, and σ_t is the allowed tensile stress. The sliding behaviour was evaluated by the following yield function f_J for sliding.

$$f_J = \tau_y - \sqrt{\tau_s^2 + \tau_t^2} = 0 \quad (14)$$

2.4 Material Parameters

To successfully apply the bounding surface plasticity model for evaluating the soil response, several soil parameters should be properly defined based on the experimental results. An experimental study in the framework of critical state soil mechanics for sands, including Toyoura sand, was conducted by Been et al. (1991) and Pradhan et al. (1989). Kawamura (1979) also conducted a series of experimental work to obtain the physical properties of saturated Toyoura sand. Most of material properties of Toyoura sand used in current analytical study was defined according to these experimental data as listed in **Table 1**.

A friction angle in the critical state ϕ_{cr} is used to define the failure surface. The value of ϕ_{cr} is approximated 31^0 for Toyoura sand (Ishihara, 1996) and the same value was assumed for both of compression and extension meridian. The parameters λ and K are the slope of the normally consolidation line and the swelling line, respectively. These values were determined by standard isotropic consolidation tests. The aspect ratio of the ellipse for the bounding surface R lies in the range of 1.5 to 3.0. In this analysis R was specified 2.25 as the typical value for sands (Crouch and Wolf, 1994b). A parameter s_e defines the elastic nucleus where only elastic strains are developed. Plastic strains are found in a very low stress level in the case of sands. In this study s_e was assumed to be one, so that the elastic nucleus shrinks to a point. The coefficient α is close to unity for most of soil-like material (Zienkiewicz, 1984). The value of coefficient α was taken to unity in this study. The hardening shape factor $h_{c1/c2}$ and $h_{e1/e2}$ control the hardening behaviour through the additive plastic modulus within the bounding surface. The hardening shape factors were determined by standard triaxial tests. These values are used for evaluating a hardening parameter h appeared in **Equation (29)** mentioned in first paper. Following formulation proposed by Wolf-Crouch (1994a).

$$h = r\, h_c \left(\frac{J}{J_1}\right)^{0.02} + \left(1 - \left(\frac{J}{J_1}\right)^{0.02}\right) \frac{h_c + h_e}{2} \quad (15)$$

$$J_1 = \frac{\varsigma_{cr} I_0}{R} \quad (16)$$

$$r = \frac{2\left(h_e / h_c\right)}{1 + \left(h_e / h_c\right) - \left(1 - \left(h_e / h_c\right)\right) \sin 3\theta} \quad (17)$$

$$h_c = h_{c1} - \left\langle 1 - \frac{IR}{I_0} \right\rangle \left(h_{c1} - h_{c2}\right) \quad (18)$$

$$h_e = h_{e1} - \left\langle 1 - \frac{IR}{I_0} \right\rangle \left(h_{e1} - h_{e2}\right) \quad (19)$$

The material properties used for a steel wall are listed in **Table 2**. Since this analytical study was conducted for very low stress level compares to yield stress level of steel, the material properties for steel wall may be defined based on elastic condition.

Table 2. Material properties of wall element

Properties	Symbol	Value	Unit
Shear Modulus	G	8.4 x 10	GPa
Poisson's Ratio	ν	0.3	
Density	ρ	7.8	g/cm^3

For the joint surface element, the material properties are defined refer to direct test performed by Hazarika and Matsuzawa (1997) [15] as given in **Table 3**.

Table 3. Material properties for interface element

Properties	Symbol	Value	Unit
Normal stiffness	k_n	44.0 x 10	GPa
Shear stiffness	k_s	22.0	GPa
Cohesion	C	10.0	kPa
Friction angle	ϕ	35.0	Degree
Allowed tensile stress	s_t	44 x 10^{-3}	MPa

Table 1. Material property for toyoura sand

Properties	Symbol	Value	Unit
Effective frictional angle	ϕ_{cr}	31	degree
Slope of isotropic consolidation Line	λ	0.02	
Slope of elastic rebound line	κ	0.002	
Parameter def. shape of ellipse	R	2.25	
Elastic nucleus parameter	s_e	1.0	
Hardening shape factor	h_{c1}/h_{c2}	0.02/0.001	
	h_{e1}/h_{e2}	0.02/0.002	
Initial void ratio	e_{in}	0.64	
Poisson's Ratio	ν	0.33	
Bulk modulus of granular soil	K_g	3.70 x 10 GPa	
Bulk modulus of pore water	K_f	2.08	GPa
Density of saturated soil	ρ	2.0	g/cm^3
Density of pore water	ρ_f	1.0	g/cm^3
Coefficient of permeability	k	1.2 x 10^{-4} m/s	
Coefficient of Contact area	α	1.0	

3. Numerical Results and Discussion

3.1 Validation of parallel computation

The numerical results at the centre of the elements behind the wall shown in **Figure 6** are discussed as the typical analysis results. In this discussion the effective stress and the pore water pressure are expressed positive for compressive. As an example, change of the lateral effective stresses, which is normal to the wall, and the pore water pressure at the point E-3, are shown in **Figure 7**. The effective stress is reduced due to the wall movement and the pore water increases at the beginning of the wall movement. These tendencies were observed in the experiment works.

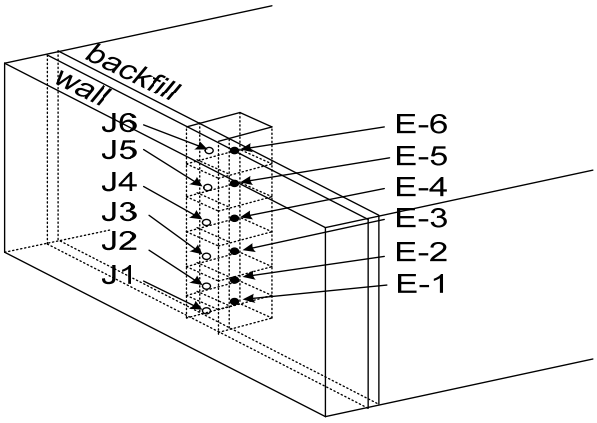

Figure 6. Position of picked up responses

Figure 8 shows the comparison of the dynamic pore water pressures acting on the wall at the point E-1 to E-6 with the experimental data. The dynamic pore water pressure corresponds with the amplitude of the pore water pressures after ten seconds excitation, i.e. when the wall movement is about 0.2 mm. The comparison plotted in **Figure 8** shows the good agreement between the analysis and the experiment.

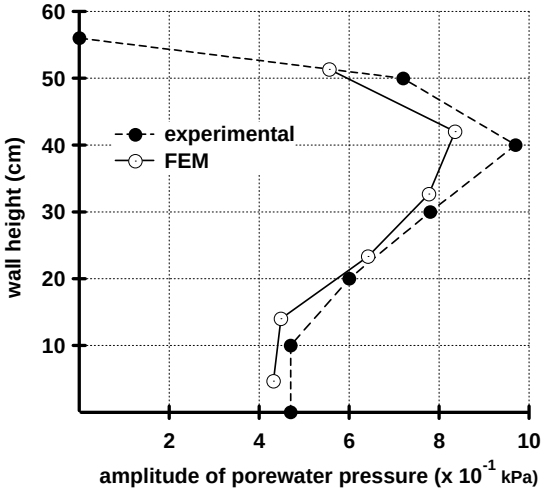

Figure 8. Comparison of the amplitude of the pore water pressure

The numerical result of the effective lateral stress distribution at the wall is shown in **Figure 9** for the wall movement 0.2 mm in which the lateral effective stresses is the maximum in the one cyclic loading. In the experiments, the lateral pressures were measured as the total force using two load cells because it is not reliable to observe the small earth pressures by the earth pressure cells. The earth pressure distribution acting on the wall was not measured directly in the experiments. The experimental values are plotted in **Figure 9** assuming the hydrostatic distribution. The total areas of the numerical results and the experimental ones are close. It is suggested the total force predicted by the analysis coincides well with the experimental one.

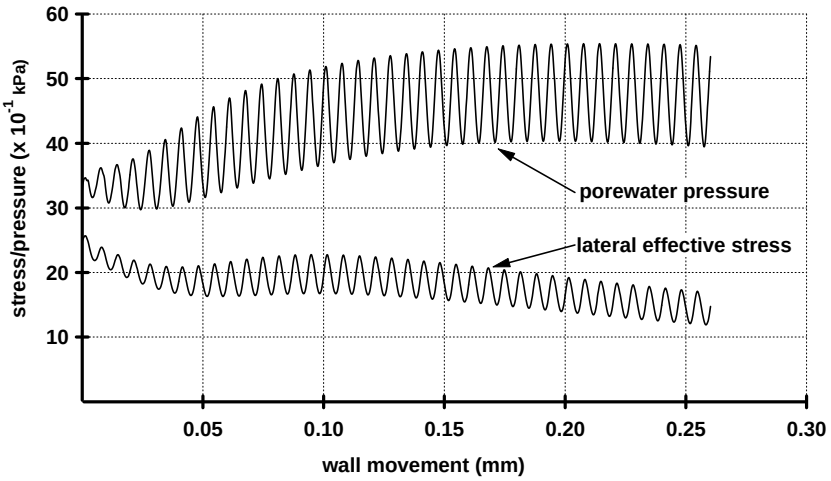

Figure 7. Effect of wall movement of lateral effective stress and pore water pressure

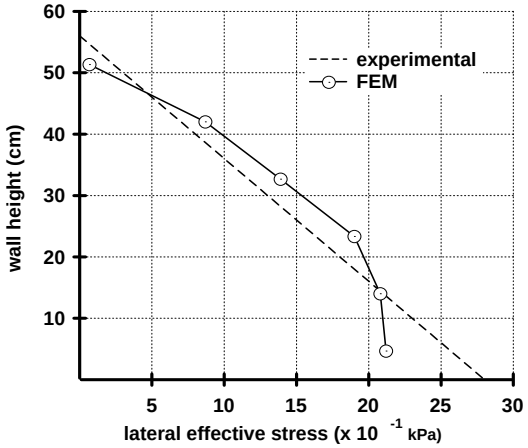

Figure 9. Comparison of the lateral pressure distribution

In the experiments the value of the lateral earth pressures was defined as the seismic active earth pressure. The slope of the experimental value in **Figure 9** represents the active earth pressure coefficient during earthquake, K_{AE}, which is applied for the current design criterion of the quay walls. The value of K_{AE} in the experiment was 0.45 and nearly equals to the value calculated by the Mononobe-Okabe equation using the seismic coefficient k_h and the density of the soil considering the effect of buoyancy. The value of K_{AE} obtained by the analysis is 0.43.

The effect of the wall movement for K and h/H are shown in **Figure 10**. K is the earth pressure coefficient for effective stresses. According to the wall movement K is reduced and h/H is also reduced at first and turned to increase after the wall movement s_m = 0.06mm. The coefficient of the wall friction f_w in the analysis is increased due to the wall movement as shown in **Figure 10.** These characteristics for K, h/H and f_w are also confirmed in the experiments.

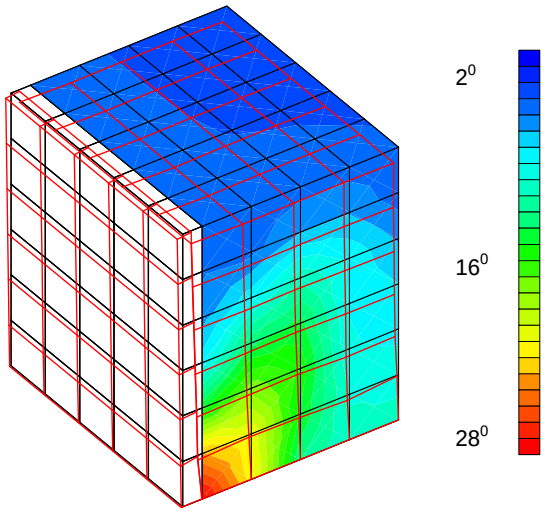

Figure 11. Deformations and failure mode of subdomain 1

The distribution of ρ_f which denotes the tangent of the mobilized angle of friction similar with ς_{cr} is shown in **Figure 11** for the subdomain **1** in the saturated soil layer and the wall movement s_m = 0.02mm. The red areas represent the stress conditions close to the critical state. The red areas starting from the bottom is presumed as a failure zone in the backfill soil. It is difficult to define the failure line in the saturated soils. In the experiment the active state where the failure occurs was defined for the wall movement s_m = 0.02mm but it is not confirmed by this numerical analysis because of the accuracy of the analysis close to the failure surface and the limitation of the infinitesimal small strain analysis.

3.2 Performance of parallel computation

To evaluate the performance of the nonlinear parallel computation, series of the analysis were carried out

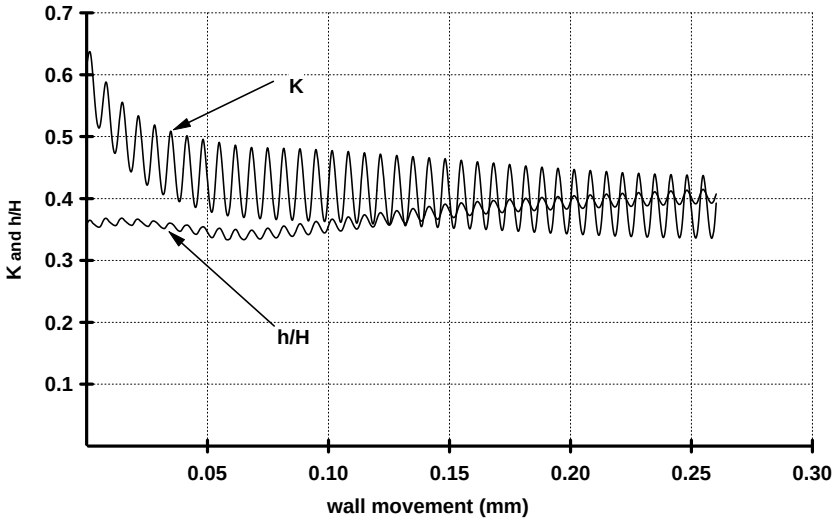

Figure 10. Responses of the earth pressure parameters

and results are shown in **Tables 4** and **5**. In the series of the analysis the results for nonlinear responses of the soil materials are compared with those of linear response of the soil material. In both of the linear and the nonlinear cases the model size and the number of processors are increased and keeping the specified number of elements assigned to one processor. The subdomain for each processor is composed of 392 elements and 3072 numbers of degrees of freedom. The executing time and the computer memory requirement were investigated as the parallel computation indicators. These indicator values were recorded after the first step of the dynamic analysis. The execution time is sum of the elapsed time for the calculation processes in each processor and the interprocessor communications. The percentage of the increment of the computer memory requirement and the executing time for each scaled model are shown in **Table 5**. For the nonlinear case, the model scaled 16 times to the original one gives the increment of the executing time and the computer memory requirement are 13.1% and 1.1%. The increment of the executing time for the linear case is 18.2%. These results suggest that the performance of the parallel computation is very efficient and more effective for nonlinear analysis rather than for the linear case.

4. Conclusions

The followings are obtained as the results of this analytical study.

1. The parallel processing FEM was applied to simulate the dynamic earth pressure problem of the saturated soil layer, which was observed in the shaking table tests and affected by the lateral movement during the excitations. The dynamic pore water pressure acting on the wall by this analysis coincides well with those of the experimental data as shown in **Figure 8**. The numerical value for the total force of seismic active earth pressures acting on the wall, which is the effective stress, was close to the experimental values as shown in **Figure 9**. The validity of the numerical results was confirmed by the comparison with the experimental data.

2. The efficiency of the parallel processing algorithm was made clear by the comparison of the executing time for different sizes of the model.

3. The 3D nonlinear parallel FEM analysis was applied successfully to the seismic active earth pressure problem first by this study. It is also first analytical study to show the relation of the effective stresses and pore water pressures in the saturated soil layer under cyclic loading and with the effect of the wall movement.

Table 4. Performance of parallel computation

Number of Processors	Problem Size	Memory (MB)	Executing Time (sec)	
			Linear	Nonlinear
1	1 x 392	5.406	71.066	204.148
2	2 x 392	5.410	75.782	206.019
4	4 x 392	5.418	80.933	212.539
8	8 x 392	5.434	82.497	225.473
16	16 x 392	5.468	84.007	230.981

Table 5. Parallel computation indicators

Scale of Model	Increment of Memory (%)	Increment of Executing Time (%)	
		Linear	Nonlinear
1	0.000	0.000	0.000
2	0.068	6.635	0.916
4	0.222	13.884	4.110
8	0.506	16.084	10.446
16	1.143	18.210	13.144

References

Beer, G., 1985, An Isoparametric Joint/Interface Element for Finite Element Analysis, *Int. Journal Num. Meth. Engg*., Vol. 21, pp.585-600.

Been, K., at.al., 1991, The Critical State of Sands, *Geotechnique*, Vol. 41, No. 3, pp. 365-381.

Crouch, R.S. and Wolf, J.P., 1994a, Unified 3D Critical State Bounding Surface Plasticity Model for Soils incorporating Continues Plasticity Loading Under Cyclic Path, Constitutive Relations, *Int. Journal Num. Anal. Met., Geomech*. Vol. 18, pp, 735-758.

Crouch, R.S. and Wolf, J.P., 1994b, Unified 3D Critical State Bounding Surface Plasticity Model for Soils incorporating Continues Plasticity Loading Under Cyclic Path, Calibration and Simulation, *Int. Journal Num. Anal. Met., Geomech*. Vol. 18, pp. 759-784.

Geist, Al. et. Al., 1996, *PVM, Parallel Virtual Machine, A User's Guide and Tutorial for Networked Parallel Computing*, Massachusetts: The MIT Press.

Hughes, T.J.R., 1996, *The Finite Element Method: Linear Static and Dynamic Finite Element Analysis*, New Jersey: Prentice Hall.

Hazarika, H. and Matsuzawa, H., 1997, Coupled Shear Band Method and Its Application to Seismic Earth Pressure Problem, Soils and Foundation, *JSSMFE*, Vol. 37, No. 3, pp. 65-77.

Ishihara, K., 1996, *Soil Behavior in Earthquake Geotechnics*, Oxford: Clarendon Press.

Kawamura, M., 1979, *Studies on Lateral Earth Pressures on Retaining Walls during Earthquakes and Heavy Rainfalls (in Japanese)*, Dissertation of Dr. Eng., Nagoya: Nagoya University.

Pradhan, B.S., at.al., 1989, Experimental Stress-Dilatancy Relations of Sand Subjected to Cyclic Loading, Soil and Foundations, *JSSMFE*, Vol. 29. No.1 pp. 45-64.

Press, W.H., et al., 1995, *Numerical Recipes in FORTRAN*, Melbourne: Cambridge University Press.

Silverio, C.J., at.al., 1994, *Fortran 77 Programmer's Guide*, Document Number 007-0711-060, Silicon Graphics, Inc.

Tanjung, J., 2010, *3D* Nonlinear Parallel FEM for Analyzing Dynamic Response of a Large-Scale Saturated Soil Layers-Civil Structures Interaction Problem (Part I: Formulation and its Numerical Solution), Bandung: *Jurnal Teknik Sipil ITB*, Vol. 17 No. 2, pp. 81-90.

Toki, K. at.al., 1981, Separation and Sliding Between Soil and Structure During Strong Ground Motion, *Earthquake Engg. Struc. Dyn*., Vol. 9, pp. 263-277.

Zienkiewicz, O.C and T. Shiomi, 1984, Dynamic Behavior of Saturated Porous Material, The Generalized Biot Formulation and Its Numerical Solution, *Int. J. Num. Anal. Meth. Geomech*., Vol. 8, pp. 71-96.